Topology optimization of cellular materials with periodic microstructure under stress constraints

Pedro G. Coelho[*], José M. Guedes[**] and João B. Cardoso[*]

[*] UNIDEMI, Faculty of Sciences and Technology
Universidade Nova de Lisboa
FCT, 2829-516 Caparica, Portugal
{pgc@fct.unl.pt, jbc@fct.unl.pt}

**IDMEC, Instituto Superior Técnico
Universidade de Lisboa
Av. Rovisco Pais 1, 1049-001 Lisboa, Portugal
{jmguedes@tecnico.ulisboa.pt}

Abstract

Material design is a critical development area for industries dealing with lightweight construction. Trying to respond to these industrial needs topology optimization has been extended from structural optimization to the design of material microstructures to improve overall structural performance. Traditional formulations based on compliance and volume control result in stiffness-oriented optimal designs. However, strength-oriented designs are crucial in engineering practice. Topology optimization with stress control has been applied mainly to (macro) structures, but here it is applied to material microstructure design. Here, in the context of density based topology optimization, well-established techniques and analyses are used to address known difficulties of stress control in optimization problems. A convergence analysis is performed and a density filtering technique is used to minimize the risk of results inaccuracy due to coarser finite element meshes associated with highly nonlinear stress behaviour. A stress-constraint relaxation technique (*qp*-approach) is applied to overcome the singularity phenomenon. Parallel computing is used to minimize the impact of the local nature of the stress constraints and the finite difference design sensitivities on the overall computational cost of the problem. Finally, several examples test the developed model showing its inherent difficulties.

Keywords Topology, Optimization, Microstructures, Convergence, Stress, Homogenization

Acknowledgements This work was partially supported by Fundação para a Ciência e a Tecnologia (Portugal) through the projects UID/EMS/00667/2013, UID/EMS/50022/2013 and PTDC/EMS-PRO/4732/2014.
Authors wish to thank Professor Krister Svanberg (Royal Institute of Technology, Stockholm, Sweden) for the MMA optimization code and Professor Hélder C. Rodrigues (IDMEC, Instituto Superior Técnico, Portugal) for all the discussions on this work.

1. Introduction

Significant improvements in industrial products have been achieved through the use of new structural materials that exhibit extreme properties found by optimal design techniques. For example, optimized composite materials have seen increased interest for lightweight construction purposes namely in automotive and aerospace industries (see, e.g., Gürdal et al. 1999).

To fully grasp the overall response of a composite one needs a greater understanding of its microstructure behaviour. A micromechanical analysis based on detailed modelling of the mixture of base constituents, often relying on homogenization techniques, is crucial to characterize its mechanical performance and to transfer the respective data across the different material length scales (see, e.g., Zohdi and Wriggers, 2005). The macroscopic behaviour of a composite is thus mechanically linked to its microstructure.

To efficiently explore the potential of composite materials, one searches for the optimal layout of its constituents within a design domain adequately parameterized and representative of the material heterogeneities (e.g., RVE, representative volume element or UC, material unit-cell). A material distribution optimization problem is then solved, targeting prescribed behaviours at the macroscopic level as design objectives or constraints. This procedure, also known as inverse homogenization, often uses density-based topology optimization (see e.g. Sigmund, 1994).

Topology optimization has been applied to design structure and material separately (single-scale models, see e.g. Sigmund and Maute 2013) as well as concurrently (multi-scale models, see e.g. Theocaris and Stavroulaki 1999, Rodrigues et al. 2002, Deng et al. 2013, Nakshatrala et al. 2013, Xia and Breitkopf 2014, Coelho and Rodrigues 2015). The basic idea is to find an optimal layout, within a particular domain, determining which spatial points should have material and which should be void (no material). The most common approach is to use density-based design variables to relax the integer nature of the original topology optimization problem transforming it into a continuous and differentiable problem solvable by gradient-based optimization methods (Bendsøe and Sigmund 2003). Although the present paper is focused on the mixture of solid and void phases (cellular materials), the formulation is readily extendable to bi-material solutions (composites).

A cellular material with periodic microstructure is studied in this work. The UC represents its smallest periodic material heterogeneity and asymptotic homogenization is used to extract the behaviour of the periodic material based on the analysis of this UC (see, e.g., Guedes and Kikuchi, 1990).

Topology optimization problems with stress based criteria are especially interesting to engineering practice because they guarantee very efficient designs and directly address aspects of material failure. However, dealing with stresses is quite challenging, mainly due to: (1) highly nonlinear stress behaviour with respect to (w.r.t.) design changes; (2) design singularity phenomenon; (3) local nature of the stress constraint(s). Topology optimization of macro-structures has developed techniques to effectively tackle these issues (see, e.g., Le et al. 2010, Deaton and Grandhi 2014). Topology optimization in material microstructure design with stress constraints has only a few contributions (see, e.g., the conference proceedings papers by Collet et al. 2016a,b). One should note the important works by Lipton and Stuebner (2005, 2006) and also recent research papers on the shape optimization of microstructures with stress control (see, e.g. Noël and Duysinx, 2017).

The primary goal of the present work is to study and optimize the topology of a material UC with stress constraints and compare (or validate) the obtained designs with literature known results. To meet this challenge, one applies current procedures, summarized below, to gain insight into the distribution of stresses within the UCs as well as to generate a well-posed topology optimization problem.

Thus, given a UC domain and the applied macroscopic stress or strain field, one computes the micro-stress distribution across the two base constituents (weaker and stronger), mixed in the UC domain, using an asymptotic based homogenization model. Typically, the stress field is highly nonlinear with design

sensitivities strongly dependent on design details. High stress gradient values are mainly located at boundary points with strong curvatures or re-entrant corners and they are very sensitive to the finite element (FE) discretization. If the accuracy of stress computation is not guaranteed, reliable designs for stress-related optimization problems cannot be expected. To overcome this, a mesh convergence analysis is performed as described in appendix A. This study further shows the benefit of using density filters in connection with square grid meshes for layout optimization with stress criteria (Sigmund 2007).

The design singularity problem means that optimal points are singular, i.e., they are located in degenerate feasible domain subspaces, which are of a lower dimension than the design space, and thus unreachable by gradient-based optimization algorithms (Cheng and Jiang 1992, Kirsch 1990, Sved and Ginos 1968). Successful stress-constraint relaxation techniques to overcome singular optima are: (1) ε-relaxation (Cheng and Guo 1997, Duysinx and Bendsøe 1998); (2) *qp*-approach (Bruggi 2008); (3) relaxed stress (Le et al. 2010, Luo and Kang 2012); (4) damage-approach (Verbart et al. 2016). Here one uses the *qp*-approach due to its straightforward implementation.

The local nature of the stress constraint implies that the optimization problem number of constraints can quickly increase with FE discretization. Thus a pointwise control of stresses based on the FE approach provides an accurate verification of stress constraints admissibility but at the expense of increasing the computational cost. A possible way to mitigate this is the use of an active set strategy where only the potentially active stress constraints are considered in each design iteration (Bruggi and Duysinx 2012). Aggregation techniques can also be used to reduce the number of local stress constraints by lumping them into a single aggregation function (Duysinx and Sigmund 1998). Regional stress measures also reduce that number (see Le et al. 2010). These later strategies decrease the computational cost but at the expense of not being able to control effectively the peak stress values. In the present work the stress constraint is imposed at each FE to avoid compromising that control.

The optimal designs shown are obtained with three-dimensional meshes, but only 2-D layouts are shown since design uniformity in one (thickness) spatial direction is imposed. The applied loads studied lead to symmetric density and stress distributions. This symmetry implies a lower number of stress-constraints since only a quarter of the UC domain is discretized. Some reference solutions can be found in the literature and are revisited here for comparison purposes.

This paper is organized as follows. In section 2 the material model is presented. The stress-based optimization problem is discussed in section 3. In section 4, stiffness and strength-oriented designs are compared. The impact of stress control on the optimal material layout is summarized in the final section 5.

2. Material Model

Consider a cellular material generated through the periodic repetition of a UC representing the smallest periodic heterogeneity of the material domain Ω, see Fig. 1. A solid and "void" phases are distributed within this UC to identify the cellular material topology. The stiffness ratio between solid and "void" phases, $E^{(1)}/E^{(2)}$, is set to 10^{12} and one assigns unitary Young Modulus to the solid phase, $E^{(1)}$=1GPa, just for demonstration purposes in the results section. Both phases are assumed linear and isotropic with Poisson ratio $\nu = 0.3$. The UC domain is Y, the volume is |Y| and its characteristic size is d. Size d is much smaller than the cellular material global size D. The behaviour of the periodic material is extracted from the UC analysis through asymptotic homogenization that assumes periodic boundary conditions on Y and infinite periodicity of the UC.

The homogenized stiffness tensor for the periodic material, E^{H}_{ijkm}, is given by,

$$E^{\mathrm{H}}_{ijkm}(\rho)=\frac{1}{|\mathrm{Y}|}\int_{\mathrm{Y}} E_{pqrs}(\rho)\left(\delta_{pk}\delta_{qm}-\frac{\partial \chi_p^{km}}{\delta y_q}\right)\left(\delta_{ri}\delta_{sj}-\frac{\partial \chi_r^{ij}}{\delta y_s}\right)\mathrm{dY} \tag{1}$$

The base material stiffness tensor E_{pqrs} depends on the topology design variable, ρ, according to the following power law (bi-material SIMP approach, see Bendsøe and Sigmund 1999),

$$E_{pqrs}(\rho) = \rho^p E^{(1)}_{pqrs} + \left(1-\rho^p\right)E^{(2)}_{pqrs}, \quad p \in \mathbf{N} \tag{2}$$

Besides a direct dependence on the base material, the homogenized stiffness tensor also depends on the UC geometry. This dependence is characterized by the micro-displacements χ^{kl} (Y-periodic), solution of the following set of equilibrium equations defined in Y (six equations in 3-D),

$$\int_{\mathrm{Y}} E_{ijpq}(\rho)\frac{\partial \chi^{kl}_p}{y_q}\frac{\partial w_i}{\partial y_j}\,\mathrm{d\,Y} = \int_{\mathrm{Y}} E_{ijkl}(\rho)\frac{\partial w_i}{\partial y_j}\,\mathrm{d\,Y}, \quad \forall_w \ \mathrm{Y-periodic} \tag{3}$$

The methodology used here to obtain the homogenized elastic coefficients in (1) and micro-displacements χ^{kl} is based on the FE software PREMAT (see Guedes and Kikuchi 1990 and Ferreira et al. 2014). The periodic boundary conditions are imposed by setting the same micro-displacements χ^{kl} values in opposite (corresponding) nodes on the UC boundaries.

The micro-stresses σ_{ij} (at the level of the material microstructure) are defined based on the micro-displacement fields χ^{rs}_k as,

$$\sigma_{ij} = E_{ijkm}(\rho)\left(\delta_{kr}\delta_{ms} - \frac{\partial \chi^{rs}_k}{\partial y_m}\right)\bar{\varepsilon}_{rs} \tag{4}$$

where $\bar{\varepsilon}_{rs}$ is the macroscopic (average) applied strain tensor, related to the macroscopic stress tensor $\bar{\sigma}_{pq}$ through

$$\bar{\varepsilon}_{rs} = C^{\mathrm{H}}_{rspq}\bar{\sigma}_{pq} \tag{5}$$

where $\mathbf{C}^{\mathrm{H}}$ is the homogenized compliance tensor computed as the inverse of the stiffness tensor $\mathbf{E}^{\mathrm{H}}$,

$$E^{\mathrm{H}}_{ijmn}(\mu)C^{\mathrm{H}}_{mnkl}(\mu) = \frac{1}{2}\left(\delta_{ik}\delta_{jl} + \delta_{il}\delta_{jk}\right) \tag{6}$$

The micro-stress field (4) represents the stress tensor field components in the UC domain Y (see also Yu and Zhang 2011). The methodology used to obtain the stress field is based on the software POSTMAT (Guedes and Kikuchi 1990). Note that the macroscopic average stress (or average strain) is assumed constant and known, corresponding to an applied uniform macroscopic tensor field.

3. Stress control in topology optimization

In this study the UC is made of a ductile base material and a von-Mises criterion is used to characterize material failure. Moreover, the UC macro loading is defined by a given strain field and the UC stiffness is bounded from below to guarantee non-trivial designs. The problem will be set as a minimum weight (volume fraction) design problem with constraints both on stiffness and local stress (see Bruggi 2016 and discussion therein for an equivalent design formulation):

$$\min_{\boldsymbol{\rho}} g_0 \quad \text{with } g_0 = V(\tilde{\boldsymbol{\rho}}) = \sum_{e=1}^{N\times N} \tilde{\rho}_e \left|\mathrm{Y}^e\right|$$

s.t.:

$$\begin{cases} g_e \le 1, \quad \text{with } g_e = \dfrac{\sigma_e^{\mathrm{VM}}(\tilde{\boldsymbol{\rho}})}{\tilde{\rho}_e^{q}\sigma^{*}} & e = 1,...,N\times N \\ g_j \le 1, \quad \text{with } g_j = 2 - \dfrac{S(\tilde{\boldsymbol{\rho}})}{S^{*}} & j = N\times N+1, \quad S(\tilde{\boldsymbol{\rho}}) = \dfrac{1}{2}\bar{\boldsymbol{\varepsilon}}\mathbf{E}^{\mathrm{H}}(\tilde{\boldsymbol{\rho}})\bar{\boldsymbol{\varepsilon}}\left|\mathrm{Y}\right| \\ 0 < \rho_{\min} \le \rho_e \le 1 & e = 1,...,N\times N \text{ and } \rho_{\min} = 10^{-3} \end{cases} \tag{7}$$

where

$$\sigma_e^{\mathrm{VM}} = \int_{\mathrm{Y}^e} \sqrt{\frac{1}{2}\left[(\sigma_{xx}-\sigma_{yy})^2 + (\sigma_{yy}-\sigma_{zz})^2 + (\sigma_{zz}-\sigma_{xx})^2\right] + 3\left(\sigma_{xy}^2 + \sigma_{yz}^2 + \sigma_{xz}^2\right)} \mathrm{d}\mathrm{Y}^e \Big/ \left|\mathrm{Y}^e\right|$$

Uniform material distribution implies uniform strain/stress distribution, and thus renders maximum stress control in the UC, constraint g_e, meaningless. The global stiffness constraint g_j is thus necessary to ensure non-uniform designs. Also in terms of mechanical design it seems appropriate to enforce concurrently stiffness and strength criteria.

In this formulation, $\tilde{\boldsymbol{\rho}}$ is the filtered density, a function of the neighbouring design variables ρ_i, as defined in Bruns and Tortorelli (2001). Assuming the density uniform in each FE, the vectors $\boldsymbol{\rho}$ and $\tilde{\boldsymbol{\rho}}$ contain the elements design variables and densities, respectively. The original design variables $\boldsymbol{\rho}$ have no physical meaning. It is the density $\tilde{\boldsymbol{\rho}}$ that defines the UC layout.

Stress distributions are computed through equations (2) and (4) for the filtered density $\tilde{\boldsymbol{\rho}}$. This helps to prevent black-white designs that exhibit jagged edges, which contain unphysical stresses (singularities). In fact, the somewhat blurred smooth boundary produced by the density filter is preferable over a sharp jagged boundary in order to smooth the local stress field and suppress unphysical singularities (see discussion in Le et al 2010). For a detailed study on the filtering effect in the stress distribution see appendix A. As an alternative solution for jagged boundary induced problems see also Svärd (2015).

The design problem constraints (7) are set as $g \le 1$, the standard form required by the MMA (Method of Moving Asymptotes, see Svanberg 1987) optimizer.

The $N\times N$ local constraints $g_e \le 1$ contain the equivalent von-Mises stress values (the average value within each element volume) within the limit value σ^*. According to Duysinx and Bendsøe (1998), the same SIMP penalization should be assumed for stiffness, p, and local stress interpolation, q, to achieve full physical consistence. However, if $p = q$ then the optimum becomes singular (Bruggi 2008). To overcome singularity one applies a suitable mathematical relaxation to the stress constraint equations, adopting an exponent $q < p$, known as the *qp*-approach (see e.g. Bruggi 2008, 2016; Bruggi and Duysinx 2012).

Additionally, the constraint $g_j \le 1$, imposes a lower bound S^* on the overall stiffness S (measured here in terms of strain energy). This is required when the loading condition is set imposing a given macro strain field $\bar{\boldsymbol{\varepsilon}}$. In the case of a given macro stress field $\bar{\boldsymbol{\sigma}}$ there is an upper bound imposed on compliance, i.e. $g_j = C/C^*$ where $C = \bar{\boldsymbol{\sigma}}\mathbf{C}^{\mathrm{H}}(\tilde{\boldsymbol{\rho}})\bar{\boldsymbol{\sigma}}\left|\mathrm{Y}\right|/2$ (see Bruggi 2016).

So, the optimal design formulation (7) aims at weight reduction, satisfying both stiffness and strength criteria. In particular, this formulation can be used to reduce stress concentrations in a standard minimum compliance optimal design. In this case, one assumes the lower bound S^* equal to the strain energy of the

optimal compliance design, while the σ^* bound is set to reduce the peak stress values. A strength-oriented optimal design can then be obtained through (7) at the expense of the UC volume fraction increase but keeping the same structural stiffness. This design approach, of reducing stress concentration in the optimal stiffness-based design, is the one pursued in this work and results are shown in the next section.

The optimizer used requires the gradients of objective and constraint functions w.r.t. the design variable ρ. When the density filter is used, the sensitivities of the objective function g_0, constraints g_e and g_j are given by (Sigmund 2007),

$$\frac{\partial g}{\partial \rho_e} = \sum_{i \in N_e} \frac{\partial g}{\partial \tilde{\rho}_i} \frac{\partial \tilde{\rho}_i}{\partial \rho_e} = \sum_{i \in N_e} \frac{\partial g}{\partial \tilde{\rho}_i} \left[\frac{R_{\min} - \left\| x_e - x_i \right\|}{\sum_{j \in N_i} \omega(x_j)} \right]; \quad \omega(x_j) = \max\left\{0, R_{\min} - \left\| x_j - x_i \right\|\right\} \tag{8}$$

where N_e defines the set of elements neighbouring element e and R_{min} is the filter radius.

Assuming a uniform density in each element and a square-grid mesh, the required derivatives w.r.t. $\tilde{\rho}$ are:

$$\frac{\partial g_0}{\partial \tilde{\rho}_i} = \left| \mathrm{Y}^e \right| \tag{9}$$

$$\frac{\partial g_e}{\partial \tilde{\rho}_i} = -\frac{q \sigma_e^{\mathrm{VM}}(\tilde{\boldsymbol{\rho}})}{\tilde{\rho}_e^{(q+1)} \sigma^*} \delta_{ei} + \frac{1}{\tilde{\rho}_e^q \sigma^*} \left(\frac{\partial \sigma_e^{\mathrm{VM}}(\tilde{\boldsymbol{\rho}})}{\partial \tilde{\rho}_i} \right) \tag{10}$$

$$\frac{\partial g_j}{\partial \tilde{\rho}_i} = -\frac{1}{2S^*} \bar{\varepsilon}_{nl} \frac{\partial E^{\mathrm{H}}_{nlkm}}{\partial \tilde{\rho}_i} \bar{\varepsilon}_{km} \left| \mathrm{Y} \right| \tag{11}$$

where $\left| \mathrm{Y}^e \right|$ is the element volume and δ_{ei} is the Kronecker symbol.

In (11), the derivative of the constitutive tensor w.r.t. density can be obtained by the adjoint method (see Bendsøe and Sigmund 2003), which for the power law (2) becomes:

$$\frac{\partial E^{\mathrm{H}}_{nlkm}}{\partial \tilde{\rho}_i} = \frac{1}{\left| \mathrm{Y} \right|} \int_{\mathrm{Y}_i} p \tilde{\rho}_i^{\,p-1} \left(E^{(1)}_{pqrs} - E^{(2)}_{pqrs} \right) \left(\delta_{pk} \delta_{qm} - \frac{\partial \chi_p^{km}}{\partial y_q} \right) \left(\delta_{rn} \delta_{sl} - \frac{\partial \chi_r^{nl}}{\partial y_s} \right) \mathrm{dY}_i \tag{12}$$

In (10), the derivative of the element von-Mises stress w.r.t. $\tilde{\rho}$ is obtained using a semi-analytical method calculated by a first-order forward finite difference,

$$\frac{\partial \sigma_e^{\mathrm{VM}}(\tilde{\boldsymbol{\rho}})}{\partial \tilde{\rho}_i} \approx \frac{\sigma_e^{\mathrm{VM}}\left[\tilde{\rho}_i (1+\alpha)\right] - \sigma_e^{\mathrm{VM}}(\tilde{\rho}_i)}{\tilde{\rho}_i \alpha} \tag{13}$$

with α as the perturbation parameter. After performing tests to assess numerical precision, $\alpha = 10^{-3}$ is chosen. When $\tilde{\rho}_i = 1$, (13) is replaced by the respective backward finite difference version. The finite difference approach is easy to implement, although computationally more costly when compared with adjoint or direct differentiation methods.

The algorithm developed to solve problem (7) is summarized in the flowchart in Fig. 2. The initialization assigns initial values to ρ followed by density filtering to obtain $\tilde{\rho}$. Homogenization (3) and local stress calculation (4) follows. Volume, stiffness and stress-constraint functions can then be evaluated. A convergence criterion is tested (e.g. iteration number, design change). If it is not satisfied one proceeds to the sensitivity analysis. The numerical gradient (8) of the von-Mises stress in each FE, with e=1,...,N×N, is evaluated in parallel. The required N^2 density perturbations are distributed through multiple core processors. Homogenization runs for each perturbation, and the corresponding stress output is used to compute the respective finite difference derivative of each stress-constraint (13). The stress, volume (9) and stiffness (11) derivatives w.r.t. design variables ρ are computed using the chain rule (8). Then, MMA updates ρ and the

density filter is applied before a new homogenization analysis is performed (with stress computation). The new $\tilde{\rho}$ is then computed and the iteration loop ends with a design convergence test.

4. Results

The accuracy of a FE model is directly dependent on the respective mesh. Density based topology optimization relies on uniform rectangular meshes. The element size (discretization level) is particularly important since one needs to warrant micro-stress evaluation quality but also to control the computational time. The FE meshes used in the following examples are chosen after convergence analysis balancing stress evaluation quality with computational time. Appendix A shows this study for the "bulk" type problem presented below.

Two different sets of examples are considered in order to test the formulation and to compare the obtained solutions with known results: a) when the average (in-plane) principal stresses/strains are of equal sign ("bulk" type); b) when they have opposite signs ("shear" type).

Case a): Average principal stresses/strains are of equal sign ("bulk" modulus type problem)

The well-known Vigdergauz-microstructures (Vigdergauz 2001, 2002) minimize both compliance and stress concentration (*e.g.* min-max von-Mises stress) provided that the *Equi-Stress Principle* (ESP) applies as the optimality condition (Banichuk 1983, Grabovsky and Kohn 1995). This is the case when one assumes the plane macro-stress $\overline{\sigma}_x = \overline{\sigma}_1$ and $\overline{\sigma}_y = \overline{\sigma}_2$ with $\overline{\sigma}_1, \overline{\sigma}_2$ of equal sign. The corresponding optimal hole shapes for different volume fractions are widely reported for the hydrostatic case ($\overline{\sigma}_1 = \overline{\sigma}_2$), see *e.g.* Vigdergauz (2001, 2002) and Noël and Duysinx (2017). The plane macro-stress case with $\overline{\sigma}_1 \neq \overline{\sigma}_2$ is reported to a much lesser extent, see *e.g.* Pederson (2000) and Bendsøe and Sigmund (1999).

As derived analytically by Grabovsky and Kohn (1995), optimal shapes of periodic holes are governed by elliptic functions with eccentricity influenced by interactions between holes. Non-interacting holes are those infinitely small and their optimal shapes become asymptotically an ellipse, $\eta = 2$ in $(x/a)^\eta + (y/b)^\eta = 1$. In this case the two half axes ratio *a*/*b* equals the stress ratio $\overline{\sigma}_1 / \overline{\sigma}_2$ and the non-zero local stresses along the hole are uniform with magnitude $\sigma_\Gamma = \overline{\sigma}_1 + \overline{\sigma}_2$ (Banischuk 1983, Lipton 1993) or $\sigma_\Gamma = \mathrm{Tr}\{\overline{\boldsymbol{\sigma}}\}/V$ with $V = 1$ in Vigdergauz (2001).

For the first example, a 100×100×1 FE mesh is used, and the following strategy is followed:

i) first a standard minimum compliance topology optimization problem with applied macro-stress field is solved with a given volume constraint,

ii) after, problem formulation (7) is solved using as constraints the previous optimal compliance value and the theoretical value for stress provided by ESP, $\sigma_\Gamma = \mathrm{Tr}\{\overline{\boldsymbol{\sigma}}\}/V$. Note that on the hole boundary, for plane stress, this is related to a constant value of the von-Mises Stress.

The results for i) and ii) are shown in Fig. 3a and Fig. 3b, respectively, for a plane macro-stress field $\overline{\sigma}_1 / \overline{\sigma}_2 = 2$, and $V = 85\%$ in i). The convergence history of the problem is shown in Fig 4. For assessment purposes, Fig. 3c shows the results obtained on a separate study, summarized in Appendix B, for similar strength and stiffness conditions, using shape optimization.

It is clear from Fig 3a that the stress distribution doesn't accurately match the ESP. In fact, the peak value of 3.707 MPa is actually above the theoretical expected value of 3.529MPa (uniform around the hole). On the other end, Fig 3b shows that introducing this stress value as the stress constraint, a more precise approximation is obtained to the known optimal shape exact solution and stress distribution (compare *a*/*b* and stress coloured scales between Fig. 3b and 3c). Note that topology is modelling the inclusion (void) as a much weaker elastic phase, where stresses become approximately zero (the blue background colour

observed). The difference of energy values between optimal topology and shape results are due to the presence of "grey" elements.

A similar comparative analysis holds for another example selected from Appendix B. An applied triaxial macro-strain ($\bar{\varepsilon}_x, \bar{\varepsilon}_y, \bar{\varepsilon}_z$) = (1.7,0.4,-0.9)×10^{-3}, equivalent to the previous plane stress in a homogeneous plate, produces the optimal topologies in Fig. 5a and 5b using the same FE mesh for stiffness and stiffness + strength designs, respectively. Note that in the last case a lower bound on stiffness *S* should be used instead of an upper bound on compliance *C*. In the topology problem the stresses are bounded by the optimal stress value obtained from shape optimization solving the min-max stress problem (Fig. 5c), as detailed in Appendix B.

Comparing the compliance and the strength-oriented topology optimization problems (see Fig 3a and 3b or Fig 5a and 5b), the volume is basically the same and energy values are equal. However, the local stress distributions around the hole and the respective peak values do not compare so well. The topology optimization problem with stress constraints reproduces the ESP and its related optimal shape with good accuracy. This means, as expected, that stress concentration is very sensitive to the geometrical design details while the total strain energy measure is rather insensitive (Pedersen 2000). This may indicate the advantage of formulating the topology optimization problem oriented also for strength.

Case b): average principal stresses/strains are of opposite sign (“shear” type)

For the shear load cases the ESP is no longer valid, however a M-equi-stress principle is satisfied (Vindergauz 2001, Noël and Duysinx 2017) for suboptimal shapes. In the following examples the density and stress results are obtained for a square-grid mesh 64×64×1. This mesh is chosen based on a mesh convergence analysis for the shear loads, similar to the one described in Appendix A. The same optimization formulation (7) is used and the following applied macro-strains are considered (plane strain):

Shear 1: in-plane distortion ($\bar{\varepsilon}_{xy} = 0.01$)

Shear 2: shear rotated 45º ($\bar{\varepsilon}_x = 0.01$, $\bar{\varepsilon}_y = -0.01$)

The shear load case 1 applies a distortion field such that stiffness *S* is maximized when a cross-shape UC is attained. As can be observed from Fig. 6, considering a volume fraction of 60%, the first design (no stress control) exhibits a square hole with sharp corners and slightly rounded sides as expected (Vigdergauz-microstructure). The change in geometry due to the imposed stress limit reveals a smaller central hole and material removed from members where the stress level was lower. The redistribution of stresses taking place approximates a fully-stressed design solution as may be expected in optimality. A significant stress reduction is achieved with a small volume fraction increase.

Equivalent von-Mises stresses are maximum at the cross arms intersections. The stress-constrained design exhibits slender holes along the cross arms and halfway from the intersections. These generated fine holes are well defined for the discretization level used and their boundaries are smooth enough so that no singularities arise.

The shear load case 2 is equivalent to the previous one but rotated by 45º. The stiffest design is also a square hole with sharp corners and slightly rounded sides but also rotated 45º, see Fig. 7a. Note that there is a scale factor ($\sqrt{2}$) between these two designs. This is a consequence of the implicit constraint imposed by the fixed UC design domain. As the stress-limit is tightened the design changes are similar to the previous example for the same range of stress limit σ^*, see Fig. 7.

In reality, these topologies recall the results obtained by Sigmund (2000) for extremal microstructures, where a square cell with square inclusions and a finer scale laminates are optimal for the bulk modulus, and

provide shear modulus for an extreme square symmetric rank2 laminate. This optimality hinges in the fact that the strain and stress fields are constant within the microstructure constituents. The obtained results show that when the stress constraint is tightened it triggers the appearance of a finer scale laminate like region, thus providing a more uniform stress field distribution.

As general comments, all these cases studied imply symmetry both in density and equivalent stress distributions. So only a quarter of the UC is modelled, reducing significantly the number of degrees of freedom, design variables and stress constraints. Note that these stress constraints should be seen as a measure of the local stress concentration factor, and do not correspond to a real stress value, since the applied average stress/strains and the Young's modulus of the UC solid part are "unitary". One also points out that an adaptive version of the stress relaxation along the iterations was implemented. This is the so-called *continuum approach* where q starts from a relative low number and gradually increases with the iteration number, i.e. as one moves toward a "0-1" design. In this work one tries not only this approach ($q = 2 \rightarrow 3$) but also q fixed to 3, with SIMP penalization $p = 4$. Both approaches proved to be equally effective when solving the examples chosen in this work. Also, the behaviour of the iteration-history curves leading to the results shown here (Fig. 4 is given as an example) offers evidence that the finite difference derivatives are accurate. Neither convergence problems nor oscillating behaviour toward the optima are detected. Finally, a speed-up of 22 is achieved here with 28 cores when solving the topology problem with stress constraints. This indicates very-good problem scalability. Note that, in problems with similar structure, parallel processing would be useful independently of the methodology used to obtain sensitivities.

5. Conclusions

Topology optimization has been extensively applied to strength design of (macro) structures, but only recently extended to material microstructure design. The primary challenges of stress control in structural optimization are non-linearity, design singularity and high computational cost due to the stress constraints local nature (Deaton and Grandhi 2014). Applications in UC material design also have to overcome these challenges. Further difficulties will appear in multi-scale design (macro/micro) due to the separation of scales in modelling heterogeneous media by asymptotic homogenization models, where micro and macro-structural descriptions are required.

This work considers optimal topology design of periodic materials UCs taking into consideration stiffness and strength requirements.

The stress field is highly non-linear and strongly dependent on the structural design. Stress levels are drastically affected by the boundary local geometric characteristics. As shown, a density filtering method has a smoothing (beneficial) effect on stresses although leading to less sharp contour between void and solid material. A crucial issue is the choice of the FE discretization assuring a robust and accurate stress field evaluation while preserving a reasonable computational cost. The mesh convergence analysis performed indicates that a UC mesh between 64×64 and 128×128 is a balanced choice.

A suitable *qp*-relaxation of the equivalent stress is used here to overcome the design singularity phenomenon. The damage approach (Verbart et al. 2016) can be explored in future developments since it relaxes the problem and simultaneously allows local stress control with just one design constraint.

The optimization problem is solved using a first-order mathematical programming method (MMA), so sensitivity analysis is required. Most of the computing effort and data storage involved are spent in the stress constraints first-order derivatives computation. The problem is worsened here since a local stress approach was taken. As a preliminary approach, finite difference approximations of the stress derivatives are used here. The obtained results show that they are reliable. Since stress-constraint derivatives can be computed independently, parallel computing techniques are used to reduce the CPU-time. Further efficiency gains can

be obtained using analytical derivatives and an appropriate treatment of the strength constraints (see Collet et al 2016a,b).

For load-bearing periodic cellular material microstructures, topology optimization can bring significant weight reduction while guaranteeing structural behaviour compliant with strength design criteria. This formulation also allows a better description of the microstructure topology, due the high sensitivity of the stress distribution to the geometrical design, expediting the satisfaction of the ESP principle for bulk macro loadings. Remarkably, in the shear macro-loading situations, peak stresses reductions of 20% to 25% are achieved with only 1 to 2% increase in UC volume fraction, this being accomplished by triggering the appearance of what seems to be an additional length scale, similar to an extremal microstructure (Sigmund 2000).

Appendix A: Mesh convergence analysis

In this study a volume fraction of 0.85 and a macro-strain ($\bar{\varepsilon}_x$, $\bar{\varepsilon}_y$, $\bar{\varepsilon}_z$) = (-1,-1,1)×10^{-2} (in-plane hydrostatic) are considered. Under these conditions the optimal topology design is a hole of circular shape (Vigdergauz 2001, 2002). The stress distributions obtained from topology optimization in square meshes (N×N×1), progressively refined, are compared to the analyses of stresses in non-square meshes specially tailored to the circular shape.

Performing optimization with a square-grid mesh without filtering technique, a jagged hole boundary is obtained (see Fig. A1a) and stress singularities appear (see Fig. A1d). If stress control is of concern this can lead to solutions that are optimal only in terms of reducing the amplitude of unphysical peak stress. This phenomenon tends to obscure more important features, in the correct solution, as the existence of a stress concentration or equi-stress state around the hole (see Fig. A1g).

So, one must ensure that the stress contours in the highly stressed areas are smooth, thus overcoming the FE jagged boundary effects. One way to promote this, while still using a square-grid mesh, is by density-based filtering techniques and mesh refinement. The results shown in Fig. A1b-c,e-f correspond to optimal compliance designs with a density filter as defined by Bruns and Tortorelli (2001).

Fig. A1b refers to a Filter = 1 meaning that the filter radius R_{min} collects for averaging only the immediate adjacent element neighbors of element i (8 neighbors in 2D, $R_{min} = \sqrt{2}/N$). Filter = 2 in Fig. A1c includes also the elements immediate adjacent to the previous neighborhood (total of 24 neighbors, $R_{min} = 2\sqrt{2}/N$). The total number of neighbors is preserved with mesh refinement thus limiting the presence of "grey" to R_{min} thickness.

The qualitative evaluation of results that can be extracted from Fig. A1 is complemented with a more quantitative one based on stress and energy values, as depicted in Fig. A2. As the mesh is refined there is strong convergence of the Strain Energy for both meshes and filters. In the maximum von-Mises stress case one sees that it deviates strongly in the case without filter, overestimating the correct solution. With the density filter one achieves a much more expectable stress distribution and accurate stress prediction (compare the colored contours in Fig. A1e-f with the tailored mesh result in Fig. A1g). For example, the stress distributions and peak values, of mesh = 64×64 with Filter = 1 (Fig. A1e) and mesh = 256×256 with Filter = 2 (Fig. A1f), mirror the reference distributions shown in Fig. A1g for the same level of discretization. The benefit of the filter in stress distribution is thus obvious. While diffusing the jagged boundary it smoothes the local stress field, suppressing unphysical singularities.

This mesh convergence analysis aims at accurate approximations of peak stresses, as they play an important role in stress-constrained optimization problems. However, the higher the accuracy the higher the computational cost. So, one also wants here to identify a mesh size that satisfactorily balances accuracy and computational resources. On one hand, since peak stresses predicted by the 64×64 and 256×256 meshes differ only by 5% one considers that convergence is attained at 64×64 discretization level. On the other hand, the computational cost becomes prohibitively high for meshes finer than 128×128. Stress-based topology optimization problems, which are typically time consuming, may become interesting to the engineering practice if one finds a reasonable trade-off between accuracy and runtime. Although the example analysed in this appendix is relatively simple, it points to a square-grid mesh with a level of discretization between 64×64 and 128×128 with the filter radius kept to a minimum, Filter = 1, as the best option. This is taken into consideration in section 4.

Appendix B: Shape optimization

A study is presented on the optimal hole's shape in a periodic perforated plate. The shape of the holes is parameterized by a super-ellipse, $(x/a)^{\eta} + (y/b)^{\eta} = 1$, where a/b and η are chosen as design variables. This has proved to be an applicable approximation for small as well as for large holes (Pedersen 2000).

The problem is formulated as the minimization of the maximum von-Mises stress, with a volume constraint, considering two load cases: (1) plane macro-stress with $\bar{\sigma}_1 / \bar{\sigma}_2$ = 2MPa/1MPa and (2) corresponding triaxial macro-strain with ($\bar{\varepsilon}_x, \bar{\varepsilon}_y, \bar{\varepsilon}_z$)=(1.7,0.4,-0.9)×$10^{-3}$ for a homogeneous plate (E=1 GPa, ν = 0.3). This problem is numerically solved using 2D quadrilateral FEs and using 3D hexahedral elements, respectively, in order to compare with topology optimization results and allowing the use of mechanically equivalent macro stress or strain. The meshes near the hole boundary are refined to warrant good results (see the example mesh in Fig. B1).

For very small holes (V≈1), the shape of an ellipse is obtained with the axis ratio a/b = 2 with both macro-fields (Banischuk 1983, Grabovsky and Kohn 1995). However, this shape quickly changes with V decrease because, on the one hand, the equivalence between the plane stress and that triaxial macro-strain is not satisfied. On the other hand, the holes interact and their optimal shapes, verifying the ESP, are given by analytical (exact) expressions not as simple as the equation of an ellipse.

At the optimal solution the exact constant stress along the hole is generally given by σ_Γ = Tr{ $\bar{\boldsymbol{\sigma}}$ }/V (see Vigdergauz 2001). In the present work, the trace is 3 and V ranges from 0.85 to 1. The peak stress value, highlighted in Fig. B1 for each V and for the applied macro-stress, directly compares well with Vigdergauz constant stress value (error < 0.5%).

The results quality in terms of attaining the ESP is measured from the maximum and minimum stress values along the design boundary and evaluating the relative error, RE = $\left|(\sigma_{\max} - \sigma_{\min})/(\sigma_{\max} + \sigma_{\min})\right| \times 100$. As V drops from 1 to 0.85, the RE increases from 0% to 5% (for both macro-fields studied). This means that nearly equi-stress boundaries are obtained in Fig. B1.

The optimal hole shape obtained for the plane macro-stress and the triaxial macro-strain with the volume fraction of 0.85 is compared to the topology optimization results shown in section 4.

References

Banichuk NV (1983) Problems and Methods of Optimal Structural Design. Plenum Press

Bendsøe MP, Sigmund O (1999) Material interpolation schemes in topology optimization. Arch Appl Mech 69:635-654

Bendsøe MP, Sigmund O (2003) Topology optimization: theory, methods, and applications. Springer

Bruggi M (2008) On an alternative approach to stress constraints relaxation in topology optimization. Struct Multidiscip Optim 36:125-141

Bruggi M (2016) Topology optimization with mixed finite elements on regular grids. Comput Methods Appl Mech Eng 3015:133-153

Bruggi M, Duysinx P (2012) Topology optimization for minimum weight with compliance and stress constraints. Struct Multidiscip Optim 46:369-384

Bruns TE, Tortorelli DA (2001) Topology optimization of non-linear elastic structures and compliant mechanisms. Comput Methods Appl Mech Eng 190(26-27):3443-3459

Cheng GD, Guo X (1997) ε-relaxed approach in structural topology optimization. Struct Optim 13(4):258–266

Cheng GD, Jiang Z (1992) Study on topology optimization with stress constraints. Eng Optim 20(2):129-148

Coelho PG, Rodrigues HC (2015) Hierarchical topology optimization addressing material design constraints and application to sandwich-type structures. Struct Multidiscip Optim 53:91-104

Collet M, Bruggi M, Noël L, Bauduin S, Duysinx P (2016a) Design of homogenized microstructures using stress-based topology optimization. In: Proceedings of 24th International Congress of Theoretical and Applied Mechanics. Montreal, Canada

Collet M, Bruggi M, Noël L, Duysinx P (2016b) Microstructural design using stress-based topology optimization. In: Proceedings of 4th European Conference on Computational Optimization. Leuven, Belgium

Deaton JD, Grandhi RV (2014) A survey of structural and multidisciplinary continuum topology optimization: post 2000. Struct Multidiscip Optim 49:1-38

Deng J, Yan J and Cheng G (2013) Multi-objective concurrent topology optimization of thermoelastic structures composed of homogeneous porous material. Struct Multidiscip Optim 47(4):583-597

Duysinx P, Bendsøe MP (1998) Topology optimization of continuum structures with local stress constraints. Int J Numer Methods Eng 43(8):1453-1478

Duysinx P, Sigmund O (1998) New developments in handling stress constraints in optimal material distribution. In: 7th AIAA/USAF/NASA/ISSMO symposium on multidisciplinary analysis and optimization. A collection of technical papers (held in St. Louis, Missouri), vol 3, pp 1501-1509

Ferreira RTL, Rodrigues HC, Guedes JM, Hernandes JA (2014) Hierarchical optimization of laminated fiber reinforced composites. Composites Structures 107:246-259

Grabovsky Y, Kohn RV (1995) Microstructures minimizing the energy of a two phase elastic composite in two space dimensions. II: the Vigdergauz microstructure. J Mech Phys Solids 43(6): 949-972

Guedes JM, Kikuchi N (1990) Preprocessing and postprocessing for materials based on the homogenization method with adaptive finite element method. Comput Methods Appl Mech Eng 83:143-198

Gürdal Z, Haftka RT, Hajela P (1999) Design and optimization of laminated composite materials. Wiley

Kirsch U (1990) On singular topologies in optimum structural design. Struct Multidiscip Optim 2(3):133-142

Le C, Norato J, Bruns T, Ha C, Tortorelli D (2010) Stress-based topology optimization for continua. Struct Multidiscip Optim 41: 605-620

Lipton R (1993) Inequalities for electric and elastic polarization tensors with applications to random composites. J Mech Phys Solids 41:809-833

Lipton R, Stuebner M (2005) Optimization of composite structures subject to local stress constraints. Comput Methods Appl Mech Eng 196: 66-75

Lipton R, Stuebner M (2006) Inverse homogenization and design of microstructure for pointwise stress control. Q J Mech Appl Math 59(1):139-161

Luo Y, Kang Z (2012) Topology optimization of continuum structures with drucker–prager yield stress constraints. Computers and Structures 90–91(0):65–75

Nakshatrala, P. B., Tortorelli, D. A., & Nakshatrala, K. B. (2013). Nonlinear structural design using multiscale topology optimization. Part I: Static formulation. Comput Methods Appl Mech Eng 261-262:167-176

Noël L, Duysinx P (2017) Shape optimization of microstructural designs subject to local stress constraints within an XFEM-level set framework. Struct Multidiscip Optim 55(6):2323-2338

Pedersen P (2000) On optimal shapes in materials and structures. Struct Multidisc Optim 19:169-182

Rodrigues H, Guedes JM, Bendsøe MP (2002) Hierarchical optimization of material and structure. Struct Multidiscip Optim 24(1):1-10

Sigmund O (1994) Materials with prescribed constitutive parameters: an inverse homogenization problem. Int J Solids Struct 31(17):2313-2329
Sigmund O (2000) A new class of extremal composites. J Mech Phys Solids 48:397-428
Sigmund O (2007) Morphology-based black and white filters for topology optimization. Struct Multidiscip Optim 33:401-424
Sigmund O, Maute K (2013) Topology optimization approaches: A comparative review. Struct Multidiscip Optim 48(6):1031-1055
Svanberg K (1987) The method of moving asymptotes - a new method for structural optimization. Int J Numer Methods Eng 24:359-373
Svärd H (2015) Interior value extrapolation: a new method for stress evaluation during topology optimization. Struct Multidiscip Optim 51:613-629
Sved G, Ginos Z (1968) Structural optimization under multiple loading. Int J Mech Sci 10:803-805
Theocaris PS, Stavroulaki GE (1999) Optimal material design in composites: an iterative approach based on homogenized cells. Comput Methods Appl Mech Eng 169(1–2):31–42
Verbart A, Langelaar M, Keulen F (2016) A new method for topology optimization with local stress constraints. Struct Multidiscip Optim 53:1081-1098
Vigdergauz S (2001) The effective properties of a perforated elastic plate numerical optimization by genetic algorithm. Int J Solids Struct 38:8593-8616
Vigdergauz S (2002) Genetic Algorithm of the effective Young moduli in a perforated plate. Struct Multidic Optim 24(2):106-117
Xia L, Breitkopf P (2014) Concurrent topology optimization design of material and structure within Fe2 nonlinear multiscale analysis framework. Comput Methods Appl Mech Eng 278:524–542
Yu N, Zhang W-M (2011) Simulating mechanical behaviour of porous materials by homogenization method. Journal of Shanghai Jiaotong University (Science) 16(2):190-194
Zohdi TI , Wriggers P (2005) Introduction to Computational Micromechanics. Springer-Verlag Berlin Heidelberg

List of Figure captions

Fig. 1 Material model of cellular material with periodic UC (array of $n \times n$ UCs in domain Ω of size D). Portray of periodic boundary conditions applied to the UC domain Y of size d

Fig. 2 Flowchart of the algorithm developed for the stress-based topology optimization in (7)

Fig. 3 Unit-cells with optimal hole geometry and respective von-Mises stresses for the plane macro-stress and V = 85%. From topology optimization: a) compliance design, b) design with stress constraints; From shape optimization: c) min-max von-Mises stress

Fig. 4 Unit-cell topology and maximum von-Mises stress along iterations (plane stress case)

Fig. 5 Unit-cells with optimal hole geometry and respective von-Mises stresses for the triaxial macro-strain and V = 85%. From topology optimization: a) compliance design, b) design with stress constraints; From shape optimization: c) min-max von-Mises stress

Fig. 6 Optimal unit-cell designs and von-Mises stress distributions for the shear load case 1. Arrays with 3×3 UCs are shown for densities above 0.85. a) Design without stress constraints; b-e) Design with stress constraints reducing progressively the peak stress from left to right (see percentage values in bold)

Fig. 7 Optimal unit-cell designs and von-Mises stress distributions for the shear load case 2. Arrays with 3×3 UCs are shown for densities above 0.85. a) Design without stress constraints; b-e) Design with stress constraints reducing progressively the peak stress from left to right (see percentage values in bold)

Fig. A1 Optimal designs obtained on top of square-grid meshes getting more refined downward (8×8, 16×16, 32×32, 64×64, 128×128, 256×256): a) no filtering; b) filter = 1; c) filter = 2. Respective von-Mises stress distributions: d) no filtering; e) filter = 1; f) filter = 2. g) Stress distribution on top of non-square grid mesh tailored to match the hole geometry

Fig. A2 Maximum von-Mises stress and Strain energy charts for the cases shown in Fig. A1, i.e. different discretizations, two meshes and three filtering options

Fig. B1 von-Mises stress distributions and their peak values for optimal super-elliptical hole shapes in periodic array. Optimal axes ratio and exponent depending on: volume fraction V [%] (99, 97, 95, 93, 91, 89, 87, 85), macro-stress ($\overline{\sigma}_x, \overline{\sigma}_y$) = (2MPa, 1MPa) and macro-strain ($\overline{\varepsilon}_x, \overline{\varepsilon}_y, \overline{\varepsilon}_z$) = (1.7, 0.4, -0.9)×10^{-3}.

Figure 1

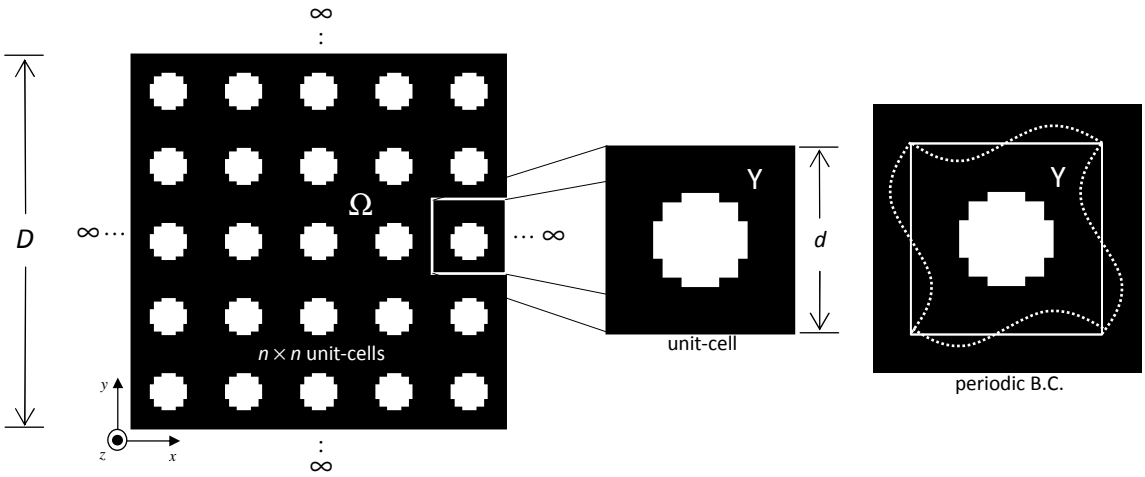

Figure 2

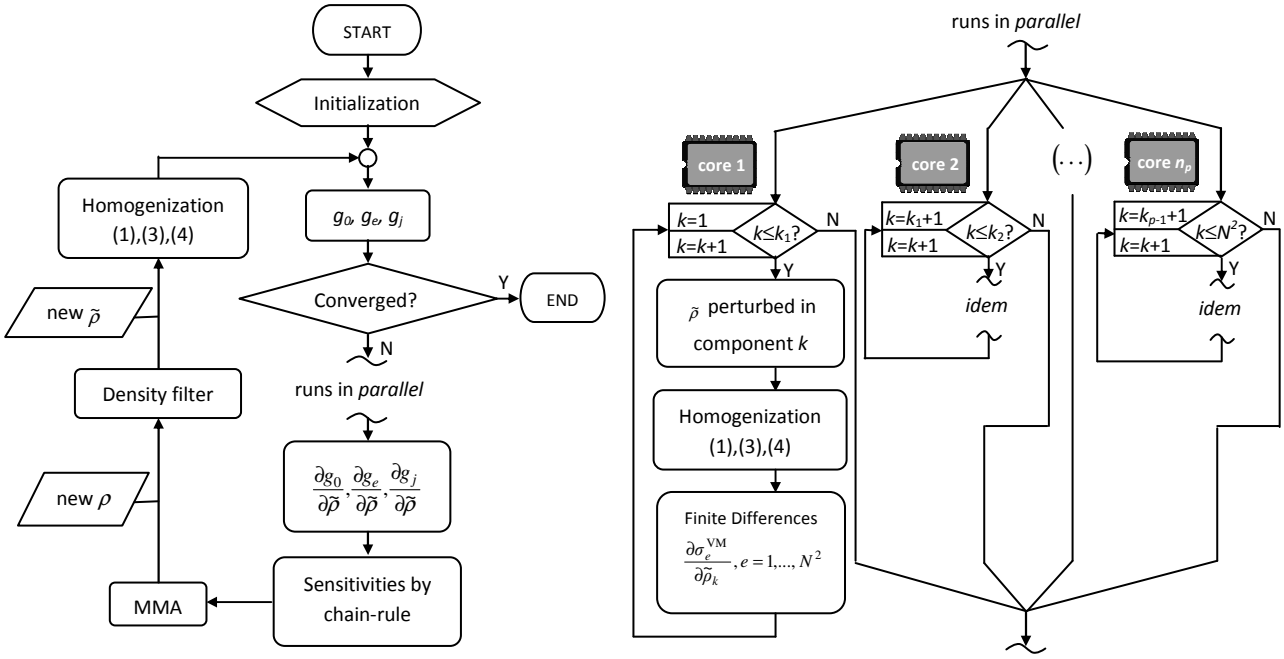

Figure 3

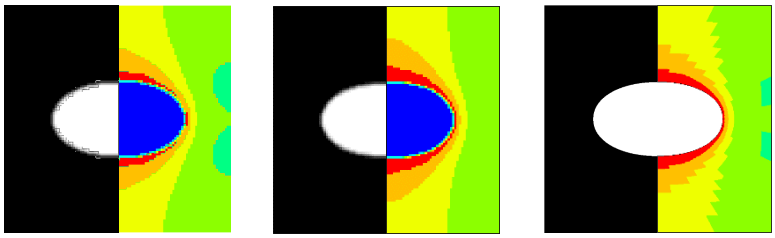

V^* = 85.00%
C = 276.29J
σ^{max} = 3.707MPa
$a/b \approx 1.750$

a)

V = 85.01%
C* = 276.29J
σ^* = 3.529MPa
$a/b \approx 1.750$

b)

V^* = 85.00%
C = 267.82J
σ^{max} = 3.546MPa
$a/b = 1.750$; $\eta = 2.121$

c)

Figure 4

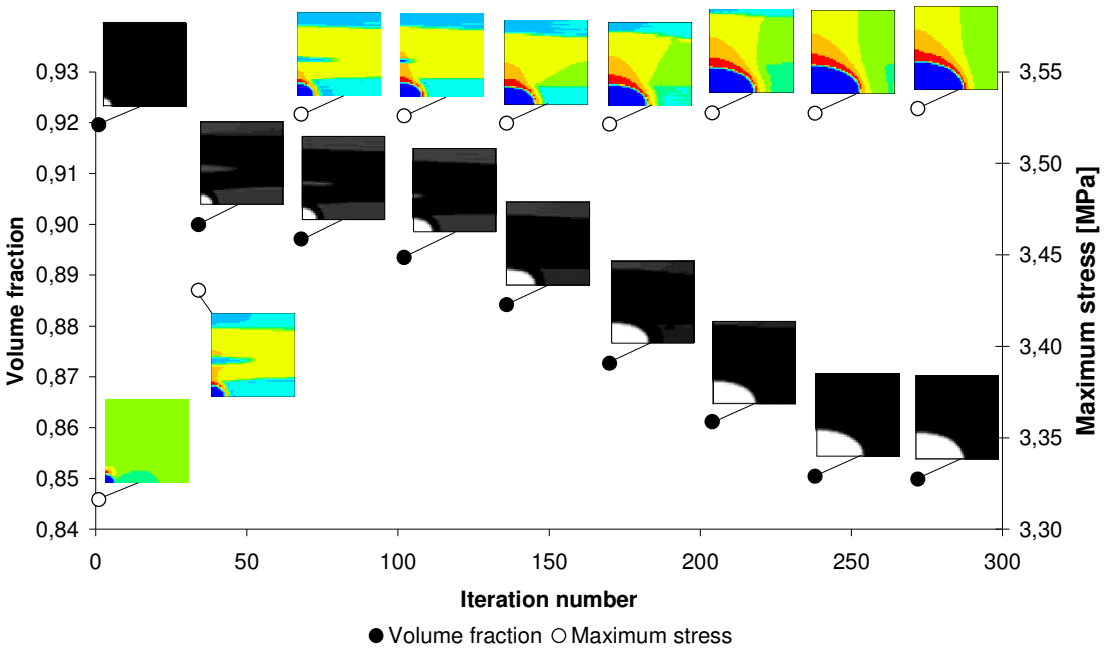

Figure 5

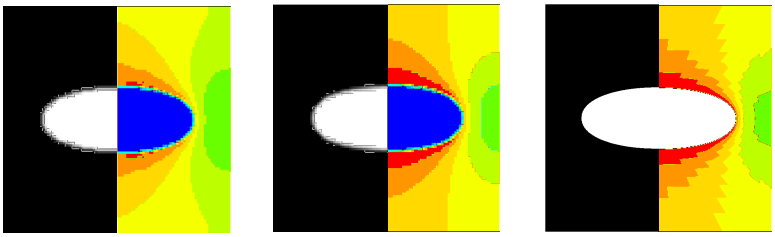

V^* = 85.00%
S = 136.15J
a)

V = 85.02%
S^* = 136.15J
b)

V^* = 85.00%
S = 139.577J
c)

Figure 6

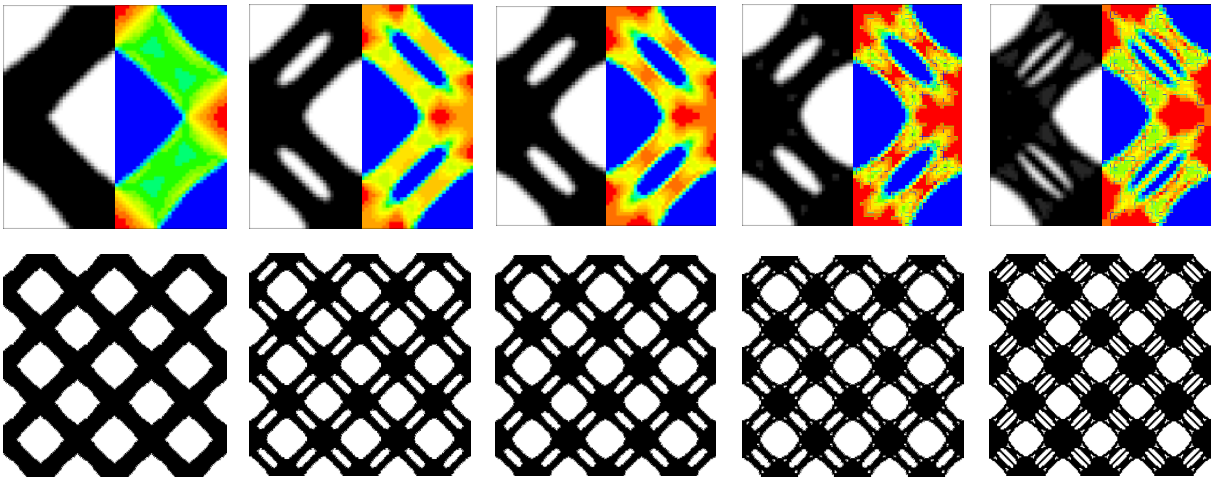

V^* = 60%
S = 3348.5J
σ^{max} = 17.19MPa
a)

V = 60.85% (+1.4%)
S^* = 3348.5J
σ^* = 13.75MPa (**-20%**)
b)

V = 61.28% (+2.1%)
S^* = 3348.5J
σ^* = 12.89MPa (**-25%**)
c)

V = 62.28% (+3.8%)
S^* = 3348.5J
σ^* = 12.05MPa (**-30%**)
d)

V = 66.78% (+11.3%)
S^* = 3348.5J
σ^* = 11.17MPa (**-35%**)
e)

Figure 7

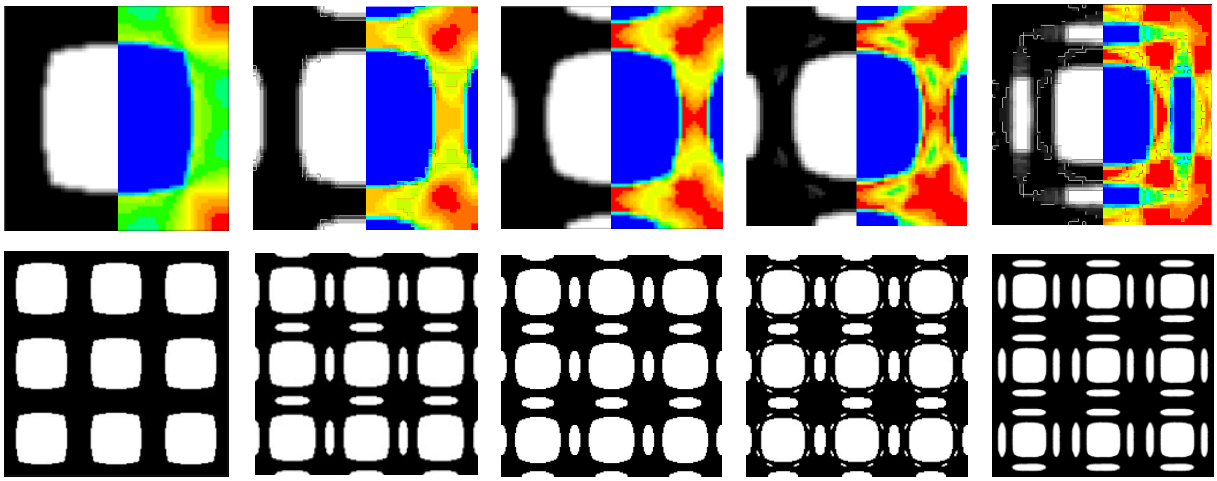

V^* = 60%
S = 3426.6J
σ^{max} = 17.09MPa
a)

V = 60.10% (+0.2%)
S^* = 3426.6J
σ^* = 13.67MPa (**-20%**)
b)

V = 60.85% (+1.4%)
S^* = 3426.6J
σ^* = 12.82MPa (**-25%**)
c)

V = 62.14% (+3.6%)
S^* = 3426.6J
σ^* = 11.96MPa (**-30%**)
d)

V = 66.49% (+10.8%)
S^* = 3426.6J
σ^* = 11.11MPa (**-35%**)
e)

Figure A1

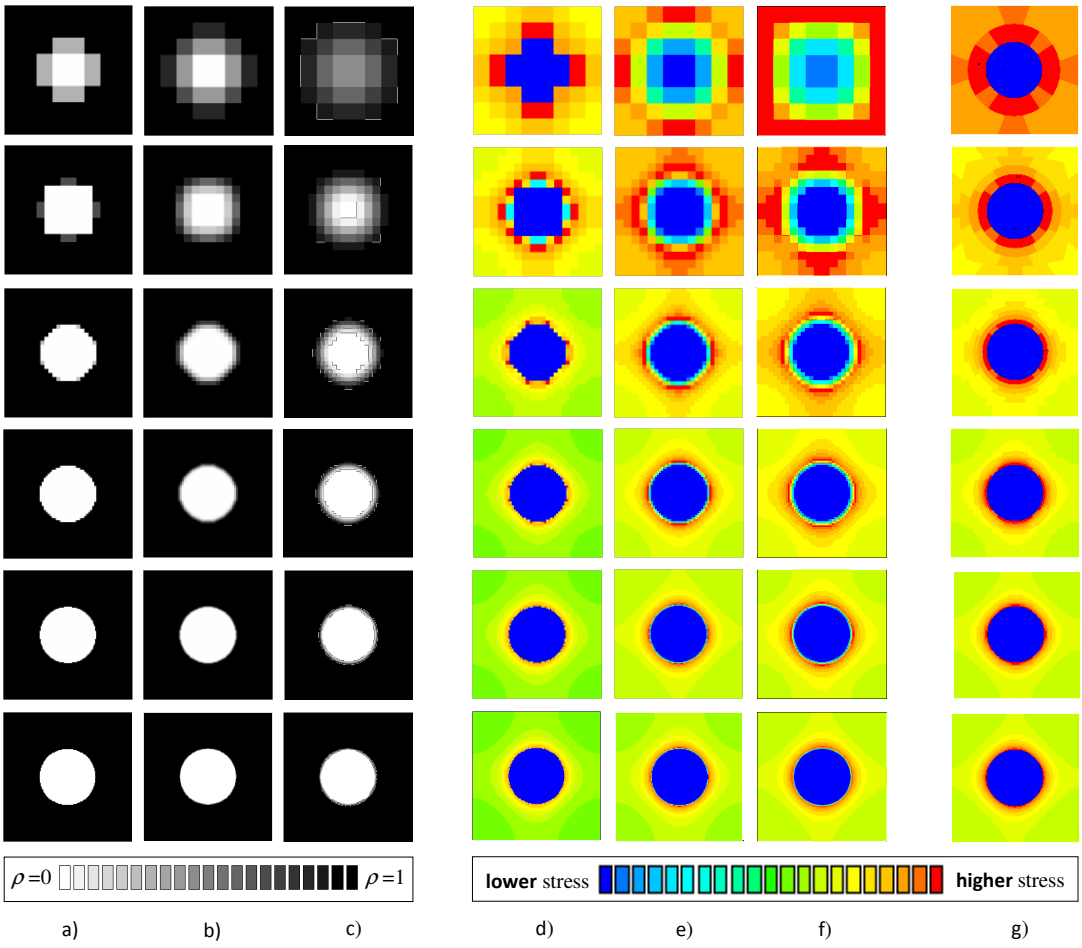

Figure A2

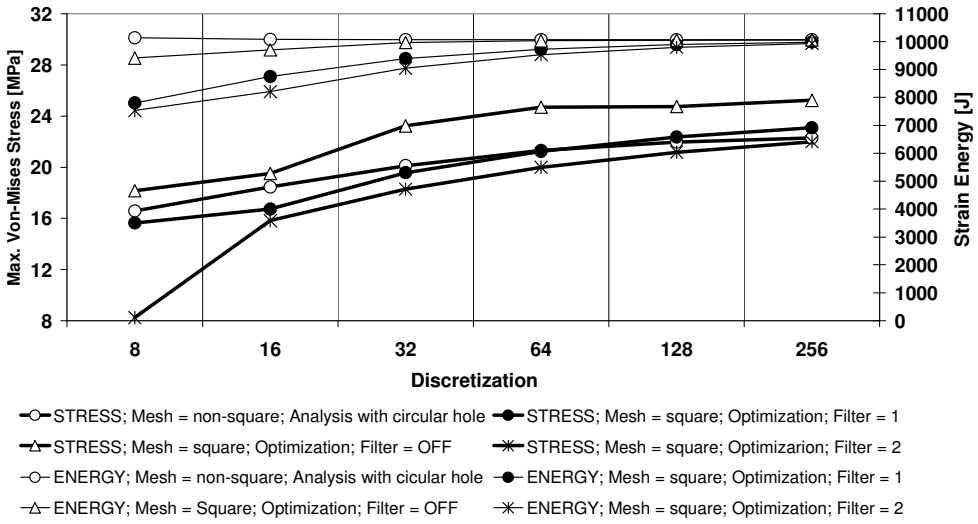

Figure B1

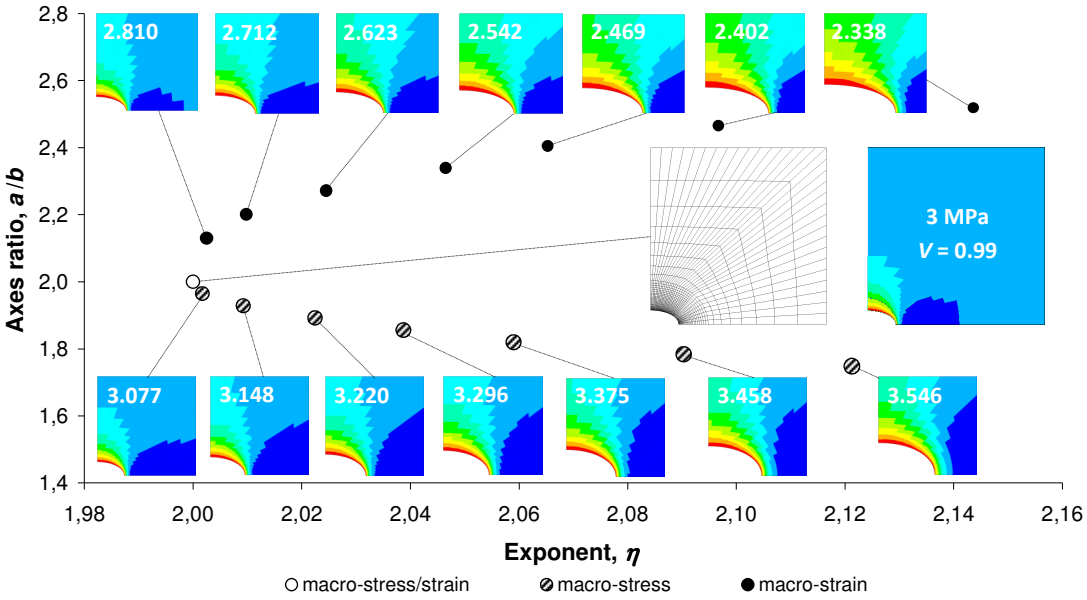
2,8
2,6
2,4
2,2
2,0
1,8
1,6
1,4
Axes ratio, a /b
1,98
2,00
2,02
2,04
2,06
2,08
2,10
2,12
2,14
2,16
Exponent, η
2.810
2.712
2.623
2.542
2.469
2.402
2.338
3.077
3.148
3.220
3.296
3.375
3.458
3.546
3 MPa
V = 0.99
macro-stress/strain
macro-stress
macro-strain